

Toward a Concordance Teleparallel Cosmology I: Background Dynamics

Mahmoud Hashim, Waleed El Hanafy,¹ Alexey Golovnev and Amr A. El-Zant

Centre for Theoretical Physics, The British University in Egypt, P.O. Box 43, El Sherouk City, Cairo 11837, Egypt

E-mail: mahmoud@aims.ac.za, waleed.elhanafy@bue.edu.eg,
alexey.golovnev@bue.edu.eg, amr.elzant@bue.edu.eg

ABSTRACT: Assuming a spatially flat universe, we study the cosmological viability of an infrared corrected teleparallel gravity model, which accounts for late acceleration by weakening gravity at later times on cosmological distances. The theory does not introduce any additional free parameters into the cosmological model, as is commonly the case with modified gravity based cosmologies. This feature renders the cosmological model statistically comparable, on equal footing, with Λ CDM. In this context, using recent cosmological observations — Pantheon supernova Type Ia, Hubble constant H_0 , Baryon acoustic oscillation, redshift space distortions, Big Bang nucleosynthesis and the cosmic microwave background constraint on the decoupling acoustic scale — we show that, although the exponential infrared-corrected gravity and Λ CDM are physically different, they are phenomenologically and statistically equivalent. However, the former is more adept at fitting accurately determined observational constraints while decreasing the H_0 tension without worsening the S_8 tension. This calls for full examination of the empirical viability of the theory at the linear perturbation level, which is the subject of paper II.

KEYWORDS: Cosmological parameters–Modified gravity

¹Corresponding author.

Contents

1	Introduction	1
2	$f(T)$ cosmology	4
2.1	$f(T)$ modification of the background dynamics	6
2.2	$f(T)$ modification of growth function	7
3	The Exponential infrared $f(T)$ Gravity	8
3.1	Motivation	8
3.2	The model	8
3.2.1	Basic form	8
3.2.2	No extra parameters	8
3.2.3	Basic properties	9
4	Observational Constraints and datasets	9
4.1	Astronomical datasets	10
4.1.1	Supernovae type Ia	10
4.1.2	H_0 measurements	11
4.1.3	Baryon acoustic oscillations	11
4.1.4	Redshift-space distortion	11
4.2	Cosmological constraints and allowed parameter space	12
4.2.1	BBN constraint on Baryon density	12
4.2.2	CMB constraints	12
4.2.3	Parameter space	12
5	Results	13
5.1	Viability of the $f(T)$ -CDM model	13
5.2	Consistency in light of various observations	14
5.3	The Hubble constant	16
5.4	The product $\Omega_m h^2$ and predicted height of CMB peak	18
5.5	Amplitude of the growth of structure	19
6	Conclusion	20

1 Introduction

Cosmological observations of Supernovae Type Ia (SNIa) distances embodied the first direct evidence for a shift from cosmic deceleration to acceleration a few billion years ago [1, 2]. This phenomenon can be accounted for through the introduction of a dark energy (DE)

component, with negative pressure, into Friedmann equation. The simplest description invokes a cosmological constant Λ , with an equation of state (EoS) fixing the ratio of pressure to density to $w_{DE} = -1$, in the field equations of general relativity (GR). Adding this to a pressureless cold dark matter (CDM) component defines the dark sector of the Λ CDM model. Although the model suffers theoretical problems, such as fine tuning [3, 4], it precisely fits a variety of cosmological and astrophysical observations. The simplicity and empirical success of Λ CDM has led to its wide acceptance, fundamental problems regarding the origin of the cosmological constant notwithstanding.

However, recent observations, with unprecedented accuracy, provide some evidence of possible physics beyond Λ CDM. A major problem involves the current value of the Hubble parameter H_0 . The cosmic microwave background (CMB) observations by Planck (base- Λ CDM) infer $H_0 = 67.4 \pm 0.5$ km/s/Mpc [5], while its most recent value according to direct local measurements using distance ladder methods (expanded sample of Milky Way Cepheids + Gaia EDR3 parallaxes) is $H_0 = 73.2 \pm 1.3$ km/s/Mpc, as measured by Riess et. al. 2020 with 1.8% precision [6, hereafter R20]. This is in 4.2σ tension with Planck (for other similar measurements see also [7–10]).

The H_0 value inferred by Planck, assuming Λ CDM, is supported by an independent dataset that combines the baryon acoustic oscillation (BAO) and big bang nucleosynthesis (BBN) with clustering and weak lensing from the Dark Energy Survey (DES) [11]. On the other hand, the late universe measurement R20 is supported by non distance ladder methods [12, 13]. And the same conclusion has been achieved by using anchors other than Cepheids to calibrate the SNIa distance ladder [14, 15]. In general, the tension between the early and the late universe of the H_0 measurements is at the 4σ –to– 6σ level for different combinations of datasets ([16], see also [17]).

The amplitude of matter fluctuations, σ_8 , provide additional evidence of tension between the early and the late universe measurements. This is often referred to as $S_8 \equiv \sigma_8 \sqrt{\Omega_m/0.3}$ tension. Here, the CMB measurements imply $S_8 = 0.834 \pm 0.016$ [5], as inferred by Planck base- Λ CDM, while cosmic shear base- Λ CDM observations from late universe give $S_8 = 0.745 \pm 0.039$ (as measured by Kilo Degree Survey [18, hereafter KiDs-450]); and $S_8 = 0.737^{+0.040}_{-0.036}$ (as measured by KiDs+VIKING-450 [19, hereafter KV-450]). These are about 2– 2.3σ lower than Planck. The preference for σ_8 values lower than Planck are obtained using redshift space distortion (RSD) observations [20, 21].

One may interpret the H_0 tension as a discrepancy in two measurements. One (early universe) measure involves the sound horizon at radiation drag r_{drag} . This being the case, one may resort to changes in early universe physics to ease the tension by reducing the sound horizon [22–25]. However, it has been shown that classical extensions of Λ CDM — such as allowing for more parameters by varying the number and masses of neutrinos — do not solve the H_0 tension on their own. They also worsen the σ_8 tension ([5]; see also [26]). On the other hand, in the extended 12 parameter space, when a dark energy equation of state $w < -1$ and neutrino species other than the standard ones are allowed to vary simultaneously, there is no preference for increasing N_{eff} when H_0 tension is addressed [27–29]. Self interacting neutrinos provide a better framework for solving both tensions simultaneously. It remains a challenge to construct and verify viable models with require-

ments beyond standard model physics with very large couplings [30, 31]. Localized energy injection around the matter-radiation equality epoch has also been invoked to reduce the sound horizon and increase the Hubble constant by introducing early dark energy [32, 33]. However, these models suffer fine tuning problems at eV scales, and also lead to severe scale dependent changes in the matter spectrum, which worsen the σ_8 tension [34]. They furthermore shift some standard Λ CDM parameters [35], in particular the spectral index n_s and the physical baryon density $\Omega_b h^2$ ($h = H_0/100$ km/s/Mpc).

A closed universe scenario was also suggested to solve some internal inconsistencies between high- $\ell > 800$ and low- $\ell < 800$ observations in the Planck data [36, 37]. However, it has been shown that when BAO is combined with Planck all parameters are enforced to flat Λ CDM even by considering the extension to 12 parameter space, which suggests even fundamentally radical extensions to the standard model need to keep the basic phenomenological elements of its success [38]. At the same line, it has been shown that the combination of Planck data with full-shape galaxy power spectrum [39] and cosmic chronometers [40] can be used to break the geometrical degeneracy, whereas the apparent preference for a closed universe from Planck disappears.

Proposals to reduce the H_0 tension through modifications of late universe physics include those invoking interacting dark matter [41], emergent dark energy [42, 43] and modified gravity [44, 45]. In particular, emergent dark energy has drawn attention as it solves the tension between CMB and local measurements of H_0 while keeping the number of free parameters exactly as in flat Λ CDM cosmology. On the other hand, an altogether different alternative explores modifications to GR on large scales.

As dark energy is a manifestation of cosmic accelerated expansion of the late universe, a suitable weakening of gravity on cosmic distances at late times may act in the same manner as dark energy, while recovering the successes of GR at early times and short distances; especially at solar system (milliparsec) scales, or binary pulsar (microparsec) scales. Such modifications may be referred to as infrared modifications of gravity (IRMG). Generally these modifications introduce new free parameters which may require further explanation and interpretation [46]. In this paper we test a particular form which does not require any. It is achieved in terms an exponential IR modification to teleparallel equivalent to GR: $f(T) = T e^{\beta T_0/T}$, where T is the teleparallel torsion scalar, $T_0 = -6H_0^2$ and β is a dimensionless parameter. The theory has been previously introduced to provide a viable dynamical phase portrait compatible with the late transition from decelerated to accelerated expansion [47]. For $\beta > 0$, GR is recovered at early times and in strong gravity regimes, where $e^{\beta T_0/T} \rightarrow 1$. Consequently, the exponential IR $f(T)$ gravity is expected to be in agreement with the CMB observations and solar system tests. It however modifies cosmic expansion on large distances at late time.

The model parameter β turns out to be completely determined by the current values of the density parameters. Therefore, unlike other viable $f(T)$ theories [48] or IRMG in general, no extra parameters are introduced relative to standard cosmology. The theory therefore does not embody, *a priori*, any additional freedom for fitting cosmological data. It is thus statistically comparable, on equal footing, with Λ CDM. In addition, this type of modification to GR acts effectively as a phantom DE without breaking the null energy

condition [49–51]. It can also completely resolve the H_0 tension between the CMB and local measurements without violating the age constraints, even if tension remains with BAO measurements [45].

In the present paper (hereafter paper I), we confront the exponential IR $f(T)$ theory with various cosmological data sets, in order to test its empirical viability. The datasets used constrain the background expansion history, as well as the growth of linear perturbations on scales well below the horizon, which turn are modified in a scale free manner. The full linear perturbation analysis of the theory, with the full CMB powerspectra using Planck 2018 legacy, will be given in a companion paper [52] (hereafter paper II). In Sec. 2, we review $f(T)$ teleparallel gravity and its effect on the cosmological background evolution. In Sec. 3, we discuss the particular $f(T)$ theory studied here. In Sec. 4, we list and discuss the observational constraints we consider, and perform the joint likelihood analysis to obtain the best-fit values for both Λ CDM and $f(T)$ -CDM models, with examining the empirical viability of the proposed $f(T)$ theory in mind. In Sec. 5, we examine the viability of the $f(T)$ gravity in light of the obtained results. In Sec. 6 we summarise our conclusions and discuss prospects for future work.

2 $f(T)$ cosmology

We consider a 4-dimensional C^∞ -manifold (\mathcal{M}, e_a) , where e_a are four linear independent vector (tetrad, vierbein) fields defined on \mathcal{M} . The vierbein fields fulfil the conditions $e_a^\mu e^\nu{}_\mu = \delta_a^\nu$ and $e_a^\mu e^\mu{}_\nu = \delta_a^\nu$, where the summation convention is assumed for both Latin (tangent 4-spacetime coordinates), and Greek (4-spacetime coordinates) [53, 54]. The spacetime metric is related to the vierbein by

$$g_{\mu\nu} \equiv \eta_{ab} e^a{}_\mu e^b{}_\nu, \quad (2.1)$$

where η_{ab} is the tangent space Minkowski metric. Moreover, one can straightforwardly construct the teleparallel geometry by finding the nonsymmetric (Weitzenböck) linear connection $\Gamma^\beta{}_{\mu\nu} \equiv e_a^\beta \partial_\nu e^a{}_\mu = -e^a{}_\mu \partial_\nu e_a^\beta$. Since $\Gamma^\beta{}_{\mu\nu}$ is nonsymmetric, it defines the torsion tensor

$$T^\beta{}_{\mu\nu} \equiv \Gamma^\beta{}_{\nu\mu} - \Gamma^\beta{}_{\mu\nu} = e_a^\beta (\partial_\mu e^a{}_\nu - \partial_\nu e^a{}_\mu), \quad (2.2)$$

while its curvature vanishes identically. Thus, in this approach, gravity is encoded in terms of torsion instead of curvature. In this teleparallel geometry, one can define the torsion scalar,

$$T = \frac{1}{4} T^\alpha{}_{\mu\nu} T^{\mu\nu}{}_\alpha + \frac{1}{2} T^\alpha{}_{\mu\nu} T^{\mu\nu}{}_\alpha - T^\alpha{}_{\mu\alpha} T^{\mu\alpha}{}_\alpha, \quad (2.3)$$

which is equivalent to the Ricci scalar R up to a total derivative term. It therefore generates the same set of field equations as GR when it replaces R in Einstein-Hilbert action. However theories representing extensions of this teleparallel equivalent to GR, known as $f(T)$ theories, differ from $f(R)$ in structure and consequences (see the review [55] for details).

Cosmological models based on $f(T)$ gravity have been extensively explored [44, 48, 56–59]. However, beyond background solutions and linear perturbations further work is required for understanding the foundational properties of $f(T)$ gravity. For, even the estimation of the number of degrees of freedom is different in different papers on Hamiltonian

analysis [60–63]. Another important foundational point relates to Lorentz invariance.. where more progress has been achieved. Unlike in the case of $f(R)$, the $f(T)$ field equations are not invariant under local Lorentz transformation in the pure tetrad (trivial spin connection) formalism [64, 65]. However, a fully covariant version of the theory can be obtained by considering the spin connection contribution to the field equations [66]. The misconception regarding their local Lorentz invariance in the $f(T)$ gravity has been also discussed in details in [54]. In addition, with regards to the propagation of gravitational waves, it has been shown that this corresponds to the speed of light, which makes such theories compatible with the observation of GW170817 and its electromagnetic counterpart GRB170817A [67], see also [68].

To evaluate the gravitational field produced by $f(T)$ gravity, we write the action

$$\mathcal{S} = \frac{1}{2\kappa^2} \int d^4x |e| f(T) + \mathcal{S}_M, \quad (2.4)$$

where $|e| = \sqrt{-g} = \det(e_\mu^a)$, the constant κ is related to the Newton’s constant G_N via $\kappa^2 = 8\pi G_N$ and \mathcal{S}_M is the action of the matter fields. The variation with respect to the vierbein gives rise to the field equations

$$\frac{1}{\kappa_{eff}^2} \mathfrak{G}_{\mu\nu} = \mathfrak{T}_{\mu\nu}^{(M)} + \mathfrak{T}_{\mu\nu}^{(DE)}, \quad (2.5)$$

where $\kappa_{eff}^2 = \kappa^2/f_T$, and we take the perfect fluid approximation to describe the matter content

$$\mathfrak{T}_{\mu\nu}^{(M)} = \rho u_\mu u_\nu + p (u_\mu u_\nu + g_{\mu\nu}), \quad (2.6)$$

where ρ , p and u^μ are the density, pressure and 4-velocity unit vector of the fluid, respectively. This defines the “geometrical” DE component via

$$\mathfrak{T}_{\mu\nu}^{(DE)} = \frac{1}{\kappa^2} \left(\frac{1}{2} g_{\mu\nu} (T f_T - f) - f_{TT} S_{\nu\mu\rho} \nabla^\rho T \right). \quad (2.7)$$

We assume the background geometry to be flat Friedmann-Lemaître-Robertson-Walker (FLRW). Hence, we take the Cartesian coordinate system $(t; x, y, z)$ and the diagonal vierbein

$$e_\mu^a = \text{diag}(1, a(t), a(t), a(t)), \quad (2.8)$$

where $a(t)$ is the scale factor of the universe. One can show that the above vierbein, via Eq. (2.1), generates the flat FLRW spacetime metric

$$ds^2 = dt^2 - a(t)^2 \delta_{ij} dx^i dx^j, \quad (2.9)$$

where the Minkowskian signature is $\eta_{ab} = (+, -, -, -)$. We note that this choice of the vierbein in Eq. (2.8) is already in the proper form, since the associated spin connection is flat and subsequently leads to symmetric field equations for any $f(T)$ theory [54] (see also [55, 66, 69, 70]). The diagonal vierbein Eq. (2.8) directly relates the teleparallel torsion scalar (Eq. (2.3)) to Hubble rate as follows:

$$T = -6H^2, \quad (2.10)$$

where $H \equiv \dot{a}/a$ is Hubble parameter, and the “dot” denotes differentiation with respect to the cosmic time t .

2.1 $f(T)$ modification of the background dynamics

The field equations corresponding to the vierbein in Eq. (2.8) give rise, respectively, to the Friedmann and Raychaudhuri equations

$$\frac{3}{\kappa^2}H^2 = \rho_m + \rho_r + \rho_T \equiv \rho_{eff}, \quad (2.11)$$

$$-\frac{1}{\kappa^2}(3H^2 + 2\dot{H}) = p_r + p_T \equiv p_{eff}. \quad (2.12)$$

The torsion density and pressure, using (2.10), in the above equations are given by

$$\rho_T = \frac{1}{2\kappa^2}(6H^2 - f + Hf_H), \quad (2.13)$$

$$p_T = -\frac{1}{6\kappa^2}\dot{H}(12 + f_{HH}) - \rho_T, \quad (2.14)$$

where $f = f(H)$, $f_H = \frac{df}{dH}$ and $f_{HH} = \frac{d^2f}{dH^2}$.

Also, we write the continuity equations of the pressureless matter (baryon + cold dark matter), radiation and the torsion (respectively)

$$\dot{\rho}_m + 3H\rho_m = 0, \quad (2.15)$$

$$\dot{\rho}_r + 4H\rho_r = 0, \quad (2.16)$$

$$\dot{\rho}_T + 3(1 + w_T)H\rho_T = 0, \quad (2.17)$$

where the torsion equation of state w_T is given by

$$w_T = \frac{p_T}{\rho_T} = -1 + \frac{(f_{HH} + 12)(f - Hf_H)}{f_{HH}(f - 6H^2 - Hf_H)}. \quad (2.18)$$

It is useful to define the effective (total) equation-of-state parameter

$$w_{eff} \equiv \frac{p_{eff}}{\rho_{eff}} = -1 - \frac{2}{3}\frac{\dot{H}}{H^2}, \quad (2.19)$$

which can be related to the deceleration parameter q by the following expression

$$q \equiv -1 - \frac{\dot{H}}{H^2} = \frac{1}{2}(1 + 3w_{eff}). \quad (2.20)$$

A nice feature of the $f(T)$ field equations is that they are of second order, unlike those associated with other gravitational theories; e.g., the $f(R)$ field equations, which are fourth order. Furthermore, this family of governing equation of any $f(T)$ theory reduces to a one-dimensional autonomous system, similar to GR. This makes the $f(T)$ gravity a natural generalization of GR, whereas the governing equation is given by [47]

$$\dot{H} = 3(1 + w)\frac{f - Hf_H}{f_{HH}} = \mathcal{F}(H). \quad (2.21)$$

This dynamical view enables the succinct visualization of the global dynamics of the system through the corresponding phase portrait in the H, \dot{H} phase-space.

2.2 $f(T)$ modification of growth function

In the framework of $f(T)$ modified gravity, at Newtonian sub-horizon scales, one can expect that the dark energy is smooth and consider linear perturbations only on the matter sector, whereas changes in the evolution of the growth of structure is determined by modified background expansion effects on the growth rate. In particular, the Hubble expansion rate H and the effective Newton's gravitational constant $\kappa_{eff}^2 = \kappa^2/f_T$; c.f. [48, 71, 72] and discussion below.

In modified gravity, generic modification of the dynamics of the linear matter perturbation at subhorizon scales can be represented via the matter continuity equation [73]

$$\Delta_m'' + \left(2 + \frac{H'}{H}\right)\Delta_m' - \frac{3}{2}\Omega_m(a)\frac{Q(a,k)}{\eta(a,k)}\Delta_m = 0, \quad (2.22)$$

for the comoving matter density perturbation Δ_m where prime denotes the derivative $d/d \ln a$ and $\Omega_m(a) = (8\pi G_N/3H^2)\rho_m$. In $f(T)$ gravity, in particular on the sub-Hubble scale, the parameters are $Q(a,k) = Q(a) = 1/f_T$ (strength of gravity modified by the factor of f_T) and $\eta(a,k) \rightarrow 1$ (no gravitational slip in the subhorizon limit, even though it is an important contribution to the superhorizon regime). Of course in case of $f(T) = T$ the standard GR is recovered.

In the present context, the evolution of the comoving density contrast Δ_m in $f(T)$ is scale independent as in GR but driven by the product $\Omega_m(a)Q(a) = \Omega_m(a)/f_T$. Therefore, in this context, $f(T)$ gravity modifies the growth of structure in a way very similar to GR. This is in contrast to $f(R)$ gravity which includes scale dependence effects. The formulation here however is valid solely at sub-horizon scale $k \gg aH$, otherwise the equation for growth has a complicated form [71, 74], which may lead to a large deviation from Λ CDM in the matter power spectra on large scales. This will be revisited in paper II [52], when the full perturbation analysis is adopted.

As linear matter perturbations in the Newtonian limit are sensitive to the background modifications through $H(a)$ and the effective Newton's constant κ^2/f_T , one can include growth rate observations in the viability test of the exponential IR $f(T)$ gravity at the background level. We define the growth factor of the matter density contrast

$$G = \frac{\Delta_m(a,k)}{\Delta_{m,0}(1,k)}, \quad (2.23)$$

where $\Delta_{m,0}(1,k)$ is the comoving density contrast current value. In practice, one considers the product $f\sigma_8$ to test the viability of the model with the red-shift space distortion observations, where the cosmological growth rate is given by

$$f = \frac{d \ln G}{d \ln a}, \quad (2.24)$$

and σ_8 is the standard deviation of the overdensity δ_m measured in spheres of radius $8 h^{-1} Mpc$. By solving Eq. (2.22) with (2.23) and (2.24), one can confront the theory with the RSD observations (see Sec. 5.5).

3 The Exponential infrared $f(T)$ Gravity

3.1 Motivation

Several $f(T)$ theories have been proposed in the literature with the aim of realizing late accelerated expansion. Such theories are generally characterized by one or two model parameters [75–77]. Under particular choices of the parameters, models that have been hitherto shown viable essentially reduce to Λ CDM cosmology but include an extra parameter relative to that standard model. This makes the latter preferable given similar fits to the data. For example in the case of the power-law theory $f(T) = T + \alpha(-T)^n$ which invokes a new independent parameter n , it has been shown that the parameter n is almost null when H_0 +SNIa+BAO+CMB dataset is used. This effectively Other $f(T)$ theories which do not cover Λ CDM as a particular case have been shown to be non-viable [48, 78].

In light of this, it becomes apparent that finding MG theories which exports α into Friedmann equation as a cosmological constant. provide a viable fundamental alternative to Λ CDM without introducing new parameters, is non-trivial. In the rest of this section, we describe one such model and outline its properties.

3.2 The model

3.2.1 Basic form

By examining the generic phase portrait patterns of viable models, an $f(T)$ theory has been proposed to produce late accelerated expansion [47]

$$f(T) = T e^{\beta(T_0/T)}, \quad (3.1)$$

where $T_0 = -6H_0^2$ and β is a dimensionless parameter.

The GR limit of this model is recovered by setting $\beta = 0$. Likewise, in the early universe and in strong gravity regimes, $T \gg \beta T_0$, the exponential correction factor goes to unity. Therefore the GR limit is recovered and no conflicts with CMB or solar system observations are expected. We now show that β is effectively entirely fixed by the matter density.

3.2.2 No extra parameters

Following [48], the modified Friedmann equation can be rewritten as

$$E^2(z) = \Omega_m(1+z)^3 + \Omega_r(1+z)^4 + \Omega_T y(z). \quad (3.2)$$

Here $E(z) = H(z)/H_0$, Ω_i is current value of density parameter (the subscript i denotes m , r and T for matter, radiation and torsion), $\Omega_T = 1 - \Omega_m - \Omega_r$, and the distortion function $y(z)$ is given by

$$y(z) = \frac{6H^2 - f(H) + Hf_H}{6\Omega_T H_0^2}, \quad (3.3)$$

where we adopted $T-H$ relation, namely Eq. (2.10). From Eq. (3.1), the distortion function becomes

$$y(z) = \Omega_T^{-1} \left(E^2 - (E^2 - 2\beta) e^{\frac{\beta}{E^2}} \right), \quad (3.4)$$

and consequently the Friedmann equation (Eq. (3.2)) reads

$$(E^2 - 2\beta) e^{\frac{\beta}{E^2}} = \Omega_m(1+z)^3 + \Omega_r(1+z)^4. \quad (3.5)$$

At the present epoch, i.e $z = 0$ and $E = 1$, the β -parameter can be expressed in terms of the current values of the density parameters as

$$\beta = \frac{1}{2} + \mathcal{W}\left(\frac{\Omega_m + \Omega_r}{-2e^{\frac{1}{2}}}\right), \quad (3.6)$$

where $\mathcal{W}(x)$ is the Lambert \mathcal{W} function¹. At present, the radiation density parameter $\Omega_r = \Omega_\gamma \left[1 + \frac{7}{8} \left(\frac{4}{11}\right)^{4/3} N_{eff}\right]$, whereas the photon density parameter $\Omega_\gamma = 2.4728 \times 10^{-5} h^{-2}$, and the effective number of neutrino species as in standard model $N_{eff} = 3.046$.

Thus the advantage of this model is that it does not introduce any new parameters in the Friedmann equation, Eq. (3.5), other than those in Λ CDM, i.e $\{\Omega_m, H_0\}$.

3.2.3 Basic properties

For larger Hubble values, the model reduces to GR. In contrast, in the small Hubble regime one expect deviations from the GR limit on large scales. This gives rise to accelerated expansion that does not necessarily correspond to that induced by a cosmological constant, while keeping GR's successes at solar system and astrophysical scales (the detailed scale dependence of this weakening is discussed in the linear regime in [52]).

At redshift $z \rightarrow -1$, one finds $E^2 \rightarrow 2\beta$. This is in fact a future de Sitter fixed point but pushed up to $t \rightarrow \infty$. Recalling Eq. (2.18), one also finds that the torsional gravity counterpart, w_T , evolves as a phantom-like DE, as probed in Fig. 1. As is well known, the infrared (IR) correction of gravity produces an apparent phantom dark energy $w < -1$ without violating the null energy condition [50, 51].

In Fig. 1 we show the general behavior of torsion acting as DE. At large z , we have $w_T(z) \rightarrow -1$, as with a cosmological constant. Nevertheless, $\rho_T = -p_T \rightarrow 0^+$, unlike a cosmological constant, which has fixed density and pressure at all time. At low redshifts $z \sim 8$, the torsional counterpart evolves as phantom DE. At present $w_T \approx -1.12$, while it is evolving towards pure de Sitter spacetime with $w_T \rightarrow -1$ as $z \rightarrow -1$ (i.e $t \rightarrow \infty$).

4 Observational Constraints and datasets

We employ different datasets to constrain the exponential IR $f(T)$ gravity, testing its viability as a model of late-time cosmic acceleration. The same analysis is applied to Λ CDM for comparison. Remarkably, in both cases, the background evolution parameters also effectively fix the parameters determining the height of the CMB peaks, while only their angular location is explicitly used here, cf. Section 5.4.

In the following subsections we give a brief description of those different datasets and the methodology used in the present analysis.

¹Defined via $x = \mathcal{W}(x) \exp \mathcal{W}(x)$.

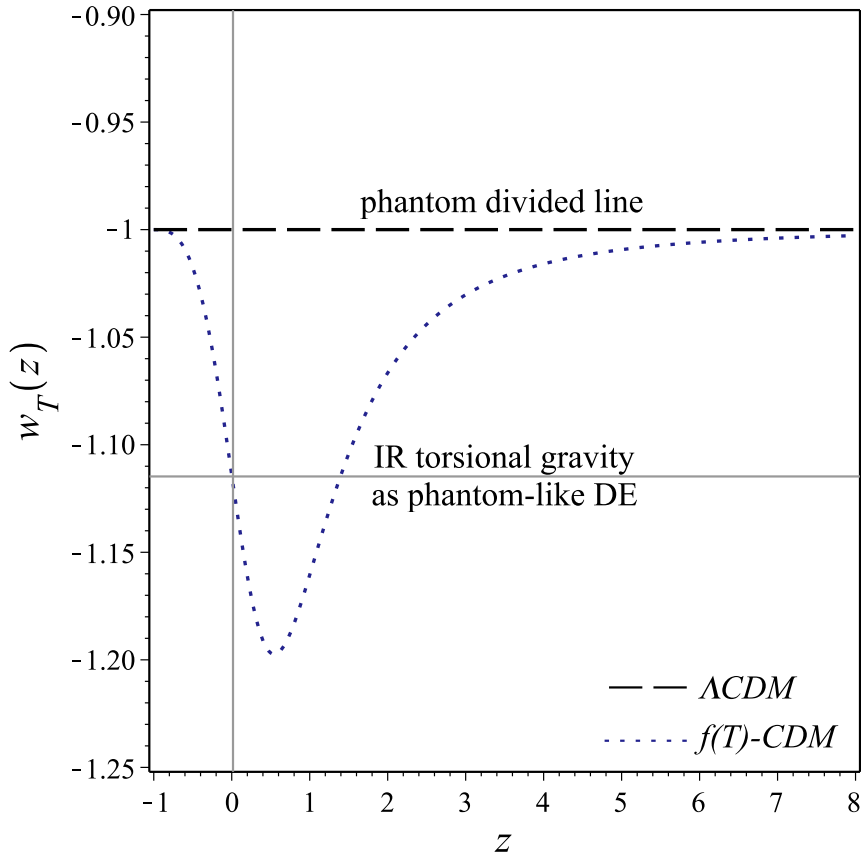


Figure 1. The evolution of torsional gravity counterpart. It illustrates the effective dark energy role and phantom-like nature of the IR gravity corrections.

4.1 Astronomical datasets

4.1.1 Supernovae type Ia

Type Ia supernovae as standard candles have been crucial to cosmology since leading to the discovery of cosmic acceleration in the late 1990's [79, 80]. In comparison with BAO and CMB data, SNIa data is however statistically less potent in constraining Λ CDM model in general. They remain nevertheless essential for testing background cosmological evolution models at low redshifts, which is the main concern of our present analysis.

The SNIa distance modulus μ is related to the luminosity distance D_L via the relation

$$\mu(z) \equiv m(z) - M = 5 \log_{10}(D_L) + 25, \quad (4.1)$$

where m is the apparent magnitude and M is the absolute magnitude. The distance D_L , in Mpc, is given by

$$D_L = \frac{(1+z)}{H_0} \int_0^z \frac{dz'}{E(z')}, \quad (4.2)$$

for a flat FLRW model (i.e. $\Omega_K = 0$). As in Eq. (4.2), the luminosity distance is solely determined by the modified Friedman equation, Eq. (3.5). To get the background dynamics

of the $f(T)$ -CDM model, we numerically solve Eq. (3.5) by iteration. Pantheon SNIa observed distance modulae are then calculated using the B-Band apparent and absolute magnitudes. The absolute magnitude M is almost constant for all supernovae and is taken as an inference parameter.

We use the Pantheon sample from [81], with 276 additional supernovae to the Joint Light-curve Analysis (JLA) sample [82–84] from the Pan-STARRS1 Medium Deep Survey, plus low-redshift and Hubble space telescope (HST) samples. This comes to a total of 1048 supernovae spanning redshift range $0.01 < z < 2.3$.

We note that from Eqs. (4.1) and (4.2), the SNIa distance modulus only constrains parameters in the function $E(z)$. This is known as distance-redshift degeneracy [85]; the absolute magnitude M is degenerate with the Hubble constant H_0 .

4.1.2 H_0 measurements

We take, as a prior, the value of the Hubble constant recently measured by a distance ladder method, using 75 Milky Way Cepheids with HST + Gaia EDR3 parallaxes, combined with best complementary sources of Cepheid calibration: $H_0 = 73.2 \pm 1.3$ km/s/Mpc with 1.8% precision [6, R20].

4.1.3 Baryon acoustic oscillations

We consider BAO radial measurements of $H(z)r_{drag}$ along the line of sight, as well as the BAO transverse measurements of $D_V(z)/r_{drag}$ perpendicular to the line of sight. Here r_{drag} is the comoving sound horizon at the end of the baryon drag, and D_V is a combination of the comoving angular distance $D_M(z) = D_L/(1+z)$ and the Hubble parameter $H(z)$ given by

$$D_V(z) = \left[D_M^2(z) \frac{cz}{H(z)} \right]^{\frac{1}{3}}. \quad (4.3)$$

We use the high precision measurements of the latest BOSS data release 12 (BOSS DR12) [86], which summarized "consensus" results on BAOs (first reported in [87, 88] and [89]) at effective redshift bins $z_{eff} = 0.38, 0.51$ and 0.61 . In addition, we consider the two measurements of D_V/r_{drag} at low redshifts $z_{eff} = 0.106$ and $z_{eff} = 0.15$ by the 6dFGS [90] and SDSS-MGS [91], respectively. We also use the WiggleZ redshift survey reconstructed measurements [92], as well as the recent BAO measurement by eBOSS DR16, using multi-tracers in configuration space, at $z = 0.77$ for $D_H \equiv c/H(z) = 19.65 \pm 0.54 \times r_{drag}$ and $D_M/r_{drag} = 18.93 \pm 0.37$ [93]. We note that, at low redshift, the combined BAO likelihood is dominated by the high precision measurements of BOSS DR12.

4.1.4 Redshift-space distortion

The peculiar motions of galaxies, relative to the Hubble flow, introduce anisotropies in the galaxy clustering observed in redshift surveys. This phenomenon is known as redshift-space distortions (RSD). The measurements of RSD could constrain the amplitude of the matter power spectrum, and in turn the structure growth rate [94]. Usually, measurements of RSD are given in terms of $f\sigma_8$, where the growth rate f is as given via (2.24). For Λ CDM,

the growth rate is approximated by the parametrization $f \sim \Omega_m^{0.55}(z)$. For the $f(T)$ -CDM model, we numerically solve Eq. (2.22) for the growth function Δ_m .

We use RSD measurements of $f\sigma_8$ from BOSS DR12 results [87], together with WiggleZ [95], eBOSS DR16 [93], SDSS MGS [96], 6dFGRS [97], and the growth rate constraint by [98] (obtained by comparing observed fundamental plane peculiar velocities in 6dFGS with predicted velocities and densities from the 2M++ redshift survey).

4.2 Cosmological constraints and allowed parameter space

4.2.1 BBN constraint on Baryon density

We use the conservative prior on the baryon density $\omega_b = \Omega_b h^2 = 0.0222 \pm 0.0005$ (68% CL), as calculated by Planck 2018 [5], and found to be compatible with the three BBN calculation pipelines based on the deuterium abundance measurement [99].

4.2.2 CMB constraints

We add a conservative CMB-BAO measurement of the angular acoustic scale at decoupling $\theta_s = \theta(z_s)$, where z_s defines the redshift at which the optical depth equals unity; i.e., $\tau(z_s) = 1$. We use the constraints on the base parameters obtained from Planck 18 (TT,TE,EE+lowE+lensing) dataset [5], to obtain the value of $100\theta_s = 1.04190 \pm 0.00030$ using the CLASS code. Since this parameter is measured with a precision of sub-percent level, the procedure allows for a tight constraint on the parameter space, comparable to those obtained from the full CMB dataset.

We note that the value derived for θ_s using the CLASS code (in the current analysis) agrees with the θ_{MC} presented in Planck results (which is derived using CAMB and CosmoMC codes) within 1σ . It is also worth mentioning that θ_s is the actual angular scale of the sound horizon at decoupling, obtained by fully integrating over the sound speed and then searching numerically for the time of decoupling (defined as the maximum of the visibility function). On the other hand, θ_{MC} is an approximation based on a model-dependent analytical fits instead of the full integral [100].

Finally, we fix two parameters as measured by CMB Planck 2018 [5], namely the optical depth at reionization $\tau(z_{re}) = 0.0544 \pm 0.0073$ and the spectral index $n_s = 0.9649 \pm 0.0042$.

4.2.3 Parameter space

For both the Λ CDM and $f(T)$ -CDM models, we take the Base dataset as SNIa + H_0 + BBN + BAO, which allows to fix three parameters, namely the Hubble parameter and the baryon and CDM densities, such that $\{H_0, \Omega_b, \Omega_c\}$. By adding the RSD data, we can fix one more parameter, that is the amplitude of the growth of structure $\{\sigma_8\}$. In addition, the inclusion of the CMB θ_s allows for better constraints on the full parameter space

$$\mathcal{P} = \{H_0, \Omega_b, \Omega_c; \sigma_8\}. \quad (4.4)$$

We also derive additional parameters, namely $\{\Omega_m, \hat{\theta}_s, r_{drag}, z_{re}, S_8\}$. Here $\hat{\theta}_s$ is the angular size of the sound horizon at recombination, z_{re} is the reionization redshift and

Table 1. 68% parameter intervals for Λ CDM and $f(T)$ -CDM models from SNIa, H_0 , BAO, BBN, RSD and CMB θ_s measurements grouped in these datasets. The minimum value of χ^2 for each model is given in the last row. Here “*Base*” represents SNIa, H_0 , BBN and BAO joint dataset.

Parameter	Λ CDM			$f(T)$ -CDM		
	Base	Base+RSD	Base+RSD+CMB θ_s	Base	Base+RSD	Base+RSD+CMB θ_s
	68% limits	68% limits	68% limits	68% limits	68% limits	68% limits
H_0	$68.3^{+1.0}_{-1.3}$	68.4 ± 1.0	68.30 ± 0.77	70.7 ± 1.3	$70.6^{+1.3}_{-1.2}$	70.52 ± 0.71
Ω_b	0.0477 ± 0.0017	$0.0477^{+0.0015}_{-0.0017}$	0.0478 ± 0.0011	$0.0438^{+0.0014}_{-0.0017}$	$0.0440^{+0.0013}_{-0.0016}$	0.04485 ± 0.00090
Ω_c	$0.256^{+0.017}_{-0.020}$	0.255 ± 0.017	0.2516 ± 0.0086	0.272 ± 0.018	0.270 ± 0.018	0.2486 ± 0.0072
σ_8	–	0.782 ± 0.024	0.781 ± 0.025	–	0.766 ± 0.033	$0.781^{+0.035}_{-0.040}$
Ω_m	$0.305^{+0.016}_{-0.018}$	0.304 ± 0.016	0.3008 ± 0.0092	0.317 ± 0.017	0.315 ± 0.017	0.2947 ± 0.0077
$100\hat{\theta}_s$	$1.044^{+0.014}_{-0.016}$	$1.044^{+0.015}_{-0.013}$	$1.04189^{+0.00030}_{-0.00033}$	$1.055^{+0.017}_{-0.015}$	$1.054^{+0.016}_{-0.014}$	1.04192 ± 0.00030
r_{drag}	$147.413^{+7.594}_{-7.626}$	$147.377^{+7.256}_{-7.387}$	$147.821^{+4.322}_{-4.981}$	$143.611^{+11.349}_{-8.026}$	$143.913^{+10.767}_{-7.88}$	$146.189^{+5.496}_{-4.385}$
z_{re}	$7.51^{+0.22}_{-0.25}$	7.49 ± 0.23	7.46 ± 0.13	7.84 ± 0.24	$7.81^{+0.26}_{-0.22}$	7.53 ± 0.12
S_8	–	0.786 ± 0.025	0.782 ± 0.025	–	0.785 ± 0.035	$0.774^{+0.035}_{-0.041}$
M	$-19.401^{+0.038}_{-0.046}$	-19.399 ± 0.037	-19.402 ± 0.021	-19.352 ± 0.047	$-19.355^{+0.047}_{-0.042}$	-19.365 ± 0.019
χ^2_{min}	519.411	523.893	525.862	516.441	518.091	524.465

$S_8 = \sigma_8 \sqrt{\Omega_m/0.3}$. In addition, to the absolute magnitude of supernova, M , taken as an inference parameter.

We use the CLASS code [100], together with Monte Python [101], after proper modifications (for the computation of $f(T)$ -CDM background dynamics) to run Monte Carlo Markov Chain (MCMC) analysis. In order to analyze the resulting MCMC chains and obtain the contour plots of the different model parameters, we use of GetDist python package [102].

5 Results

In this section we test the viability of the $f(T)$ -CDM theory with a full likelihood analysis and compare it to Λ CDM. We also examine the consistency of the obtained results in light of the different datasets listed and described above. We point out the recent tensions between different datasets and discuss prospects for resolution within the exponential IR $f(T)$ theory.

5.1 Viability of the $f(T)$ -CDM model

As the current $f(T)$ theory has the same number of free parameters as Λ CDM model, a direct statistical comparison using a χ^2 is straightforward.

In Table 1, we list the best-fit values up to 68% CL, for both Λ CDM and the exponential IR $f(T)$ theory, using different combinations of cosmological datasets; such as Base (\equiv SNIa+ H_0 +BBN+BAO), Base+RSD and Base+RSD+CMB θ_s . As can be seen, the minimum Chi-squares (χ^2_{min}) for both models are comparable, with slight preference for $f(T)$ in all dataset combinations, which confirms the viability of the $f(T)$ -CDM model. We note that by utilizing the concise CMB measurement of the angular scale of the sound

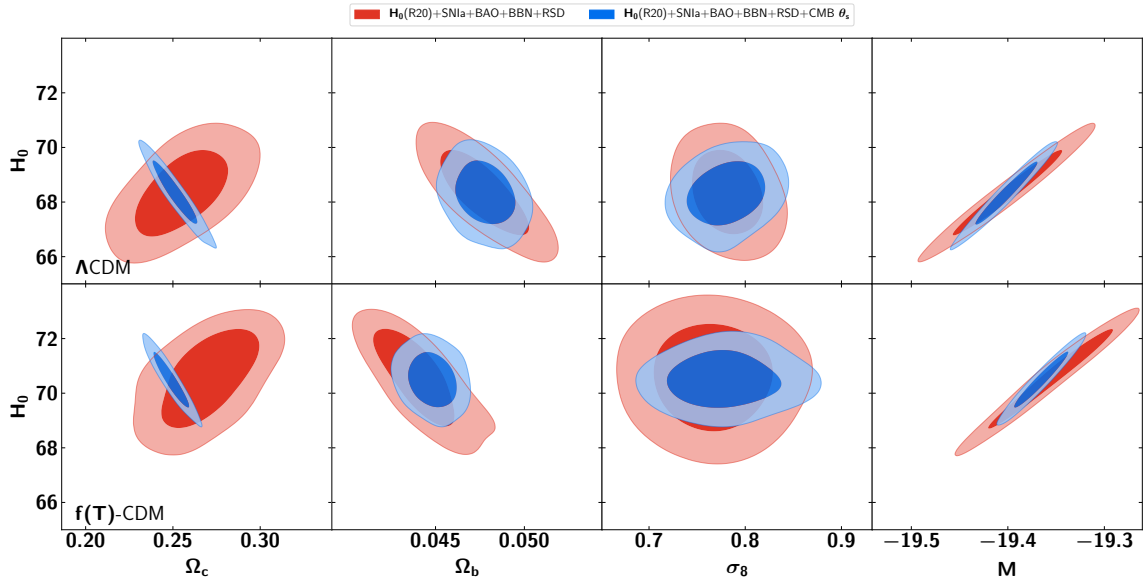


Figure 2. A compilation of 1σ and 2σ contour plots for the CDM and baryon density parameters, the nonlinear scale fluctuations σ_8 , and the supernovae magnitude M (as inference parameter), against H_0 . This is shown for both Λ CDM, in the upper panel, and $f(T)$ -CDM model, in the lower panel. Red contours represent the joint likelihood analysis for SNIa, $H(z)$, BAO, BBN and RSD datasets, while blue contours include in addition the BAO measurement of the CMB (namely the angular acoustic scale θ_s measurement).

horizon, θ_s , we obtain more constrained values of the inferred parameters, while keeping the agreement of the two models within 1σ .

In Fig. 2, we plot the 2D joint contours of the model parameters $\{\Omega_c, \Omega_b, \sigma_8\}$ versus H_0 , for Λ CDM and $f(T)$ -CDM scenarios at 68% and 95% confidence level (CL). This was done using the full likelihood analysis for the full set of parameters, including the inferred ‘nuisance’ parameter M , for two main datasets (with/without CMB θ_s constraint). As is apparent, with the inclusion of the Planck constraint on the CMB θ_s , both Λ CDM and $f(T)$ -CDM remain in agreement, while the latter gives higher H_0 value compared to Λ CDM, indicating a partial solution of the associated tension.

5.2 Consistency in light of various observations

We examine the consistency of the obtained results from the joint MCMC likelihood with individual observational datasets; namely how they fare separately with SNIa, BAO and RSD. We use the best fit values, in particular the full dataset combination Base+RSD+CMB θ_s , as provided by Table 1 for both the Λ CDM and the exponential IR $f(T)$ models.

In the upper panel of Fig. 3, Pantheon data are compared with Λ CDM and $f(T)$ -CDM models with best-fit parameters values. Both are in a good agreement with SNIa data. We note that the Λ CDM and $f(T)$ -CDM models give, respectively, absolute magnitudes $M = -19.402 \pm 0.021$ and $M = -19.365 \pm 0.019$ which are close to the true absolute magnitude

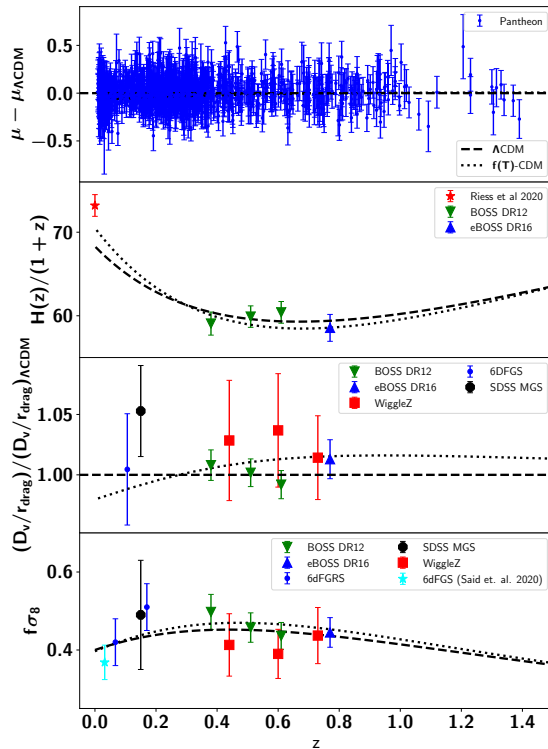


Figure 3. Various datasets are compared with theoretical predictions of Λ CDM and $f(T)$ -CDM models, as given in Table 1. Upper panel: Residual of SNIa distance modulus measurements (blue dots) of Pantheon data sample from Λ CDM model. Second panel: Hubble parameter H_0 from R20 local measurements (red star), BOSS DR12 BAO radial distance measurements (green down triangles) and eBOSS DR12 (blue up triangle). Third panel: the ratio of D_V (Eq. 4.3) over the comoving sound horizon at the baryon drag r_{drag} , with respect to Λ CDM model from BOSS DR12 (green down triangles), WiggleZ (red squares), eBOSS DR12 (blue up triangle), low redshift 6DFGS (blue dot) and SDSS MGS (black pentagon) measurements. Bottom panel: $f\sigma_8$ measurements from the same dataset as in the third panel in addition to 6dFGRS (blue dots) and the recent 6dFGS measurement (cyan star) [98].

of SNIa, $M = -19$.

In the second panel of Fig. 3, we show how well Λ CDM model fits $H(z)$ BAO measurements, as provided by the precise constraints of BOSS DR12 and the recent eBOSS DR16 observations over redshift range $0.3 < z < 1$. However, it fails to reach local measurement of H_0 value at $z = 0.0$ [9]. On the other hand, $f(T)$ -CDM tends to reach higher H_0 value in better agreement with the local H_0 measurement while keeping the good fit with the BAO $H(z)$ measurements.

In the third panel of Fig. 3, we plot various BAO data used in this analysis in comparison with the theoretical prediction from $f(T)$ -CDM model. We show the distance of the acoustic-scale ratio D_V/r_{drag} at several effective redshifts (as given in the figure), divided by the acoustic-scale ratio in the Λ CDM model. Both Λ CDM and $f(T)$ -CDM (with best fit parameters) seem to agree very well with BAO measurements. We note that the expo-

nential IR $f(T)$ gravity entails a relatively mild phantom regime later in cosmic expansion history relative to the power law models discussed in [45]. Additionally, the current treatment only partially alleviates the H_0 tension. In this context, the stark inconsistencies with BAO distances found in the aforementioned work are avoided.

In the bottom panel of Fig. 3, we use the best fit values of Table 1 to plot the theoretical predictions of the rate of the growth of structure diagnostic $f\sigma_8$ for Λ CDM and $f(T)$ -CDM models. Both models seem to agree perfectly with the RSD dataset.

Another consistency test of the exponential IR $f(T)$ gravity is the age of the universe as predicted by the theory. According to the full likelihood results, as given in Table 1, the age of the universe is ~ 13.76 Gyr, which is not in conflict with any of the known astrophysical observations so far [103–105].

We conclude that the exponential IR $f(T)$ theory is statistically similar to Λ CDM, since both have the same number of free parameters, and the best-fit χ^2 results are almost the same for the different dataset combinations in Table 1. The $f(T)$ theory however shows some deviations at low redshifts as clear from Fig. 3 with $H(z=0)$ and $f\sigma_8$. We focus on the tensions related to these quantities in the following.

5.3 The Hubble constant

As is already clear from Table 1, the best fit values in parameter space for Λ CDM and the $f(T)$ -CDM model are recognizably different when the CMB θ_s is absent from the joint MCMC analysis (namely the Base and the Base+RSD combined data). However, the inclusion of the CMB θ_s results in consistent values for the two models. This is understandable, as the angular acoustic scale is observationally pinpointed with $\sim 0.03\%$ precision.

In order to further examine how Λ CDM and $f(T)$ -CDM fit the Planck CMB measurements, we plot the $\hat{\theta}_s$ - z_s 2D joint contours for both models. As can be seen from Fig. 4, the models provide slightly different values of $\hat{\theta}_s$ at recombination in absence of the CMB θ_s , with a slight preference of $f(T)$ gravity with Planck constraints. On the other hand, both fit well with Planck constraints at the recombination epoch, introduced by including the Planck constraint on the CMB θ_s . In this case both models have similar early history and deviations in the derived parameters are due to late time evolution.

Despite the similar contours, the small changes still lead to discernible differences in parameters. Using the full likelihood For Λ CDM we obtain $H_0 = 68.30 \pm 0.77$ km/s/Mpc, which is 3.2σ lower than the R20 local measurement $H_0 = 73.2 \pm 1.3$ km/s/Mpc [6]. On the other hand, for $f(T)$ -CDM we obtain $H_0 = 70.52 \pm 0.71$ km/s/Mpc using the same dataset, which is 1.8σ lower than the local measurement; i.e. the $f(T)$ -CDM is closer to the R20 measurement than Λ CDM by 1.4σ , while keeping similar χ^2_{min} for the full dataset. Thus, the analysis shows the Planck constraint on the CMB θ_s fixes the early history of the two models similarly but allows the exponential IR $f(T)$ theory to better fit with local H_0 measurements.

In order to understand how these models take different tracks in the late universe, it is convenient to compare their Friedmann equations, in the matter domination era. For

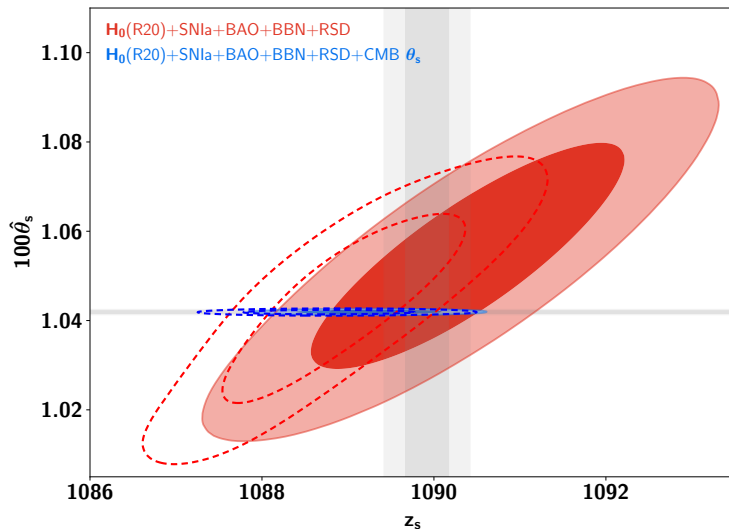


Figure 4. Constraints on $100\hat{\theta}_s-z_s$: Solid contours are for $f(T)$ -CDM and dashed contours are for Λ CDM model; grey bands represent 1σ and 2σ constraints from CMB Planck 2018 on the acoustic scale and the redshift at recombination [5]. In absence of any constraint from the CMB θ_s , i.e. the red contours, the $f(T)$ -CDM theory predicts an acoustic scale a little bit different from Λ CDM predictions. This deviation can be understood in terms of slight different evolutions at late time, as clear in Fig. 3. However, by including an the precise CMB θ_s constraint, i.e. the blue contours, it similarly fixes the early time evolution of both models in agreement with Planck measurements within $\sim 1\sigma$.

general dynamical dark energy or modified gravity models, we write Friedmann equation

$$E(z) = H(z)/H_0 = \sqrt{\Omega_m(1+z)^3 + \Omega_{de}y(z)},$$

where

$$\Omega_{de} = 1 - \Omega_m \text{ and } y(z) = e^3 \int_0^z \frac{1+w_{de}(z')}{1+z'} dz'.$$

In the particular case of Λ CDM, $w_{de} = -1$, we obtain $y(z) = 1$. However, in the phantom dark energy with fixed equation of state $w_{de} < -1$, we obtain $y(z) = (1+z)^{3(1+w_{de})}$ which finds $y(0) = 1$ and $y(z > 0) < 1$ in a systematic way as z goes higher. This clearly shows that how phantom energy lowers the expansion rate $E(z)$ at $z > 0$ relative to Λ CDM, which in return increases the angular diameter distance to the last scattering surface $D_A(z_s) = (1+z_s)^{-2}D_L(z_s)$ while keeping the early universe unaltered (in particular the sound horizon r_s). Nevertheless the CMB angular scale of the first peak $\theta_s(z_s) = r_s(z_s)/D_A(z_s)$ can be restored to its measured value by accommodating larger H_0 value. Similar argument can be applied in the case the exponential IR $f(T)$ -CDM which effectively imposes dynamical phantom dark energy $-1.2 \lesssim w_{de} \lesssim -1$ at late $z \lesssim 8$, see Fig. 1.

Fig. 5 shows the the relevant contours in the H_0 - Ω_m plane, reflecting consistently larger allowable H_0 values for the $f(T)$ model relative to Λ CDM. On the other hand, by adding CMB θ_s prior, the $f(T)$ -CDM keeps higher H_0 values while slightly decreases not only the mean value of Ω_m but also decreases its 1σ and 2σ compared to Λ CDM predictions of Ω_m .

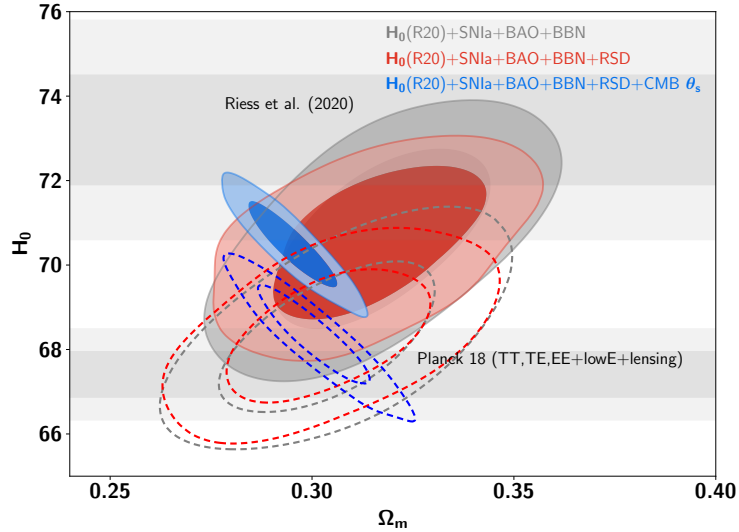


Figure 5. Constraints in the H_0 - Ω_m plane: Solid contours are for the $f(T)$ -CDM model, while dashed contours are for Λ CDM. The upper grey bands represent 1σ and 2σ levels of the local measurement of H_0 from R20, while the lower bands represent 1σ and 2σ of Planck 2018 H_0 constraints. As is apparent, when adding the CMB θ_s constraint, $f(T)$ -CDM tends closer to R20 H_0 value (which partially alleviates the H_0 tension), while Λ CDM model, as expected, circumscribes H_0 values similar to Planck 2018.

This shows that the $f(T)$ -CDM prediction of Ω_m is more constrained when the CMB θ_s is considered. These changes still need to be examined with the well measured value $\Omega_m h^2$ known as the geometric degeneracy as provided by the CMB power spectrum.

5.4 The product $\Omega_m h^2$ and predicted height of CMB peak

We note that the CMB angular acoustic scale θ_s used in these calculations is related to the location of the first acoustic peak of the temperature anisotropy of the CMB power spectrum [106–108]. The height of the acoustic peak, on the other hand, is constrained by the matter density $\Omega_m h^2$. This was, in principle, left as a free parameter in our analysis. But the best fits to both models considered here result in values remarkably close to the measured one. According to Planck 18 base- Λ CDM, this physical matter density $\Omega_m h^2 = 0.1430 \pm 0.0011$ [5]. The full likelihood Base+RSD+CMB θ_s predicts $\Omega_m h^2 = 0.1403 \pm 0.0053$ for Λ CDM — lower than Planck by $\sim 0.5\sigma$ — and $\Omega_m h^2 = 0.1466 \pm 0.0048$ for $f(T)$ -CDM, which is higher than Planck by $\sim 0.7\sigma$.

Thus the two models are interestingly in agreement with Planck within 1σ error using mainly late universe observations and just the location of the first peak — without involvement of the full CMB power spectrum. This is a reflection of a consistency, once labelled concordance, in values of the parameters inferred from different routes. The term concordance has come into disuse, in large part in light of the progressively exacerbating H_0 tension. This tension however is alleviated to some extent in the context of our present $f(T)$ model without introducing extra parameters.

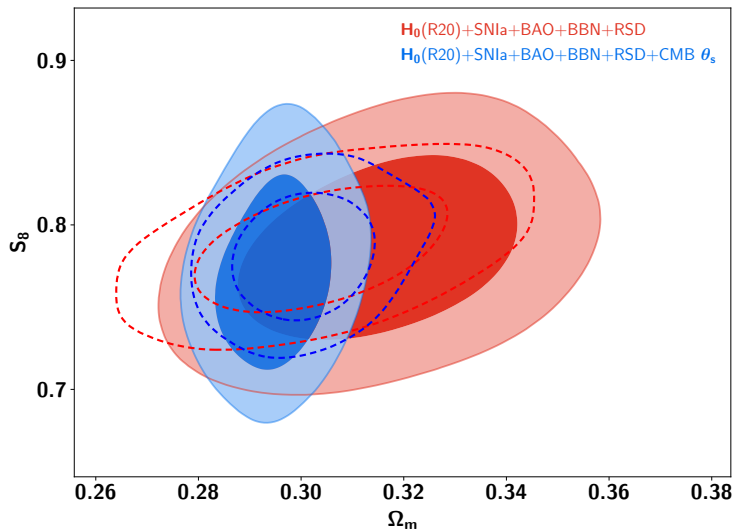


Figure 6. Constraints at 68% and 95% CL on S_8 – Ω_m plane: Solid contours are for $f(T)$ -CDM model, while dashed contours are for Λ CDM. The 2D contour plots show that both models give comparable results with slightly smaller S_8 value within the $f(T)$ -CDM scenario. This shows that the exponential IR $f(T)$ gravity does not worsen S_8 tension in comparison to the Λ CDM model. However, full investigation requires us to derive the S_8 value, at the linear perturbation level of $f(T)$ -CDM theory, as inferred by CMB powerspectrum too and to compare it with late universe measurements. This is shown in paper II [52].

5.5 Amplitude of the growth of structure

Another late universe dataset that is in tension with Λ CDM-Planck is the cosmic shear measurement of the matter fluctuation by Kilo Degree Survey 450 (KiDs-450). For the flat Λ CDM model, the matter amplitude $S_8 = \sigma_8 \sqrt{\Omega_m/0.3} = 0.834 \pm 0.016$ at 68% CL, as measured by the CMB alone (TT,TE,EE+lowE) [5]. In contrast, the corresponding value, as measured by KV-450 is $S_8 = 0.737^{+0.040}_{-0.036}$, when using Λ CDM with a prior on H_0 from direct measurements [19]. The tension between those measurements is thus above 2σ . Any suggested model to reconcile the early and the late H_0 measurements should not strengthen the tension in other measurements like S_8 .

Recalling the discussion about the $f(T)$ modification of growth function and the RSD measurements in Subsections 2.2 and 4.1.4, respectively, whereas the growth rate in $f(T)$ scenario is given by Eqs (2.22), (2.23) and (2.24) while the RSD observations measure the product $f\sigma_8$. Therefore, by extracting the amplitude σ_8 and consequently the S_8 parameter, we plot the two dimensional S_8 – Ω_m plane for both Λ CDM and exponential IR $f(T)$ -CDM models using the joint likelihood without/with CMB θ_s constraint as obtained in Fig. 6. It is obvious that the 2D contour plots for both Λ CDM and $f(T)$ -CDM models are compatible within 1σ regions.

In more detail, using the Base+RSD data without(with) CMB θ_s constraint, we respectively obtain $S_8 = 0.786 \pm 0.025$ (0.782 ± 0.025) for Λ CDM and slightly smaller $S_8 = 0.785 \pm 0.035$ ($0.774^{+0.035}_{-0.041}$) for $f(T)$ -CDM which are in agreement with the cosmic shear

Λ CDM-base measurement $S_8 = 0.737^{+0.040}_{-0.036}$ at 68% CL as provided by KV-450. In addition, both predict almost same σ_8 values as obtained in Table 1, which indicates that the exponential IR $f(T)$ gravity does not- in principal- worsen the S_8 -tension.

Although we restrict ourselves to linear matter perturbation in the Newtonian limit (well below horizon scales), a full analysis is not expected to modify the aforementioned conclusions, as significant modifications in its context would arise on scales much larger than those affecting than those associated with the S_8 tension. In order to investigate the S_8 -tension within the IR $f(T)$ gravity we need to derive its value as inferred by Planck full CMB and KiDs-450 (or KV-450) cosmic shear, simultaneously, and then we can properly check their consistency. This requires the extension of our analysis to the full linear perturbation effects. We leave such a fuller examination to paper II [52].

In sum, at the background level, we find that the $f(T)$ -CDM theory (3.1) can fit well with different types of observations. It is statistically similar to Λ CDM and it can serve as a viable theory of gravity, while providing a framework for reducing tensions between early and late universe with H_0 and tentatively does not worsen S_8 . Although, the exponential IR $f(T)$ theory and Λ CDM are conceptually different, they share the same number of free parameters and are statistically similar in viability in terms of the tests undertaken here.

6 Conclusion

Late accelerated expansion is a crucial issue of unclear origin in contemporary cosmology. The range of possibilities is unconstrained in such a way as to allow for a cosmological constant, dynamical dark energy or modified gravity as sources for the phenomenon. If one assumes the latter option, IR corrections to gravitational theories may represent a viable scenario; as they modify gravity on cosmic distances while keeping GR predictions fulfilled on smaller scales, such as the solar system scales where it is very well tested. In this context, the exponential IR $f(T) = T e^{\beta T_0/T}$ gravity was proposed in Ref. [47], its dynamical phase portrait was examined and shown to account for late time acceleration. Here, we examined in detail the empirical viability of the consequence of that model on the background dynamics of cosmic expansion; confronting it with various datasets, covering widely spaced epochs and scales of the Universe.

As the theory does not introduce any extra free parameters compared to Λ CDM, it allows for statistical comparison on equal footing. This is unlike other viable $f(T)$, or modified gravity theories in general, which usually include at least one extra free parameter. This being the case, one need not resort to such techniques as performing Bayesian information criteria ($\text{BIC} = -2 \ln L^{\text{max}} + n \ln m$) to obtain well grounded comparisons — since n (number of parameters) and m (number of data points) are the same for both models, and only the maximum likelihood L^{max} (i.e. χ^2_{min}) affects the results. As Λ CDM is already very successful in fitting available data, modified gravity models that improve on those fits by adding tiny modifications through extra parameters are likely to be associated with worse BIC, especially when the number of data points is not so large, c.f. [78]. Furthermore, marginalizing over extra parameters has the effect of enhancing the H_0 tension by broaden-

ing the uncertainties of its inferred value rather than an actual shift of the H_0 mean value [31]. Such issues are avoided here.

We used SNIa, H_0 , BAO, RSD, BBN, and CMB θ_s to examine the viability of the theory. We evaluated the joint likelihood analysis to find the best-fit values of the four model's parameters $\{H_0, \Omega_b, \Omega_c, \sigma_8\}$ for both Λ CDM and $f(T)$ -CDM models. After appropriate modification of CLASS code with Monte Python, we ran MCMC samples. Then, we used GetDist python package to analyze MCMC chains and get the 2D contour plots at 1σ and 2σ regions of the different model parameters.

The comparison clearly illustrates that $f(T)$ -CDM and Λ CDM show similar statistical success when confronted with the various datasets. Moreover, while including the accurate CMB constraint θ_s , the $f(T)$ -CDM theory makes it possible to decrease the H_0 tension by 1.4σ relative to the Λ CDM prediction using the dataset presented in this study, while still giving an age for the universe (~ 13.76 Gyr), compatible with other astrophysical observations.

The product $\Omega_m h^2$, on which depends the height of the first CMB peak is left free in our analysis, which uses late universe data, in addition to the angular location from θ_s . Nevertheless, the measured value is obtained within $1\text{-}\sigma$ for both models. This is reflection of a consistency between parameter values obtained from different routes. Once termed concordance, the term has come into disuse, partly due to the progressively serious H_0 tension. As mentioned, this tension is less serious in the context of the teleparallel-based cosmology presented here.

The exponential IR $f(T)$ gravity considered here drives the effective equation of state to slip significantly into the phantom regime at lower redshifts, as in the models studied in [45]. Significant deviations from Λ CDM are milder and occur later than those associated with the inverse power-law $f(T)$ discussed there however. This allows the exponential IR $f(T)$ to be in less severe tension with BAO measurements, in particular the angular distance, while partially alleviating the H_0 tension. In the present study, this alleviation arose as a compromise statistical optimum fitting the various datasets. Larger tensions with the BAO distances may be expected if full resolution between CMB and local H_0 measurements is required.

Although we were mainly concerned with constraints arising from the background evolution, we have included the effect on the growth on linear perturbations on (Newtonian) scales significantly smaller than the horizon, as the effect turns out to be scale free in the linear regime. In this context, constraints from redshift space distortion suggest that the exponential IR $f(T)$ gravity leads to slightly smaller $S_8 = \sigma_8 \sqrt{\Omega_m/0.3}$, while keeping σ_8 almost the same as for Λ CDM. This indicates that the exponential IR $f(T)$ gravity does not worsen the tension associated with the normalization of the amplitude of fluctuations. In a companion paper we perform a full perturbation analysis and compare the results with the CMB spectrum.

The IR correction approach is not limited to $f(T)$ teleparallel gravity, which should be primarily seen as an example of how modified gravity models can successfully explain the late accelerated expansion by weakening the gravity on the cosmic distances. Although $f(T)$ cosmology is generally simpler to handle mathematically, a major challenge

concerns extending its predictions to the non-linear regime of structure formation, ultimately attempting to adopt it to N -body simulations, in order to fully test its viability and consequences.

Acknowledgements

This project was supported financially by the Science and Technology Development Fund (STDF), Egypt. Grant No. 25859. The likelihood analysis presented in this work were done on the Sciama High Performance Compute (HPC) cluster which is supported by the ICG, SEPNet and the University of Portsmouth.

References

- [1] A.G. Riess, A.V. Filippenko, P. Challis, A. Clocchiatti, A. Diercks, P.M. Garnavich et al., *Observational Evidence from Supernovae for an Accelerating Universe and a Cosmological Constant*, *The Astronomical Journal* **116** (1998) 1009 [[astro-ph/9805201](#)].
- [2] S. Perlmutter, G. Aldering, G. Goldhaber, R.A. Knop, P. Nugent, P.G. Castro et al., *Measurements of Ω and Λ from 42 High-Redshift Supernovae*, *Astrophys. J.* **517** (1999) 565 [[astro-ph/9812133](#)].
- [3] S. Weinberg, *The Cosmological Constant Problem*, *Rev. Mod. Phys.* **61** (1989) 1.
- [4] S.M. Carroll, *The Cosmological constant*, *Living Rev. Rel.* **4** (2001) 1 [[astro-ph/0004075](#)].
- [5] PLANCK collaboration, *Planck 2018 results. VI. Cosmological parameters*, [1807.06209](#).
- [6] A.G. Riess, S. Casertano, W. Yuan, J.B. Bowers, L. Macri, J.C. Zinn et al., *Cosmic Distances Calibrated to 1% Precision with Gaia EDR3 Parallaxes and Hubble Space Telescope Photometry of 75 Milky Way Cepheids Confirm Tension with LambdaCDM*, [2012.08534](#).
- [7] A.G. Riess et al., *A 2.4 Determination of the Local Value of the Hubble Constant*, *Astrophys. J.* **826** (2016) 56 [[1604.01424](#)].
- [8] A.G. Riess, S. Casertano, W. Yuan, L. Macri, J. Anderson, J.W. MacKenty et al., *New Parallaxes of Galactic Cepheids from Spatially Scanning the Hubble Space Telescope: Implications for the Hubble Constant*, *Astrophys. J.* **855** (2018) 136 [[1801.01120](#)].
- [9] A.G. Riess et al., *Milky Way Cepheid Standards for Measuring Cosmic Distances and Application to Gaia DR2: Implications for the Hubble Constant*, *Astrophys. J.* **861** (2018) 126 [[1804.10655](#)].
- [10] A.G. Riess, S. Casertano, W. Yuan, L.M. Macri and D. Scolnic, *Large Magellanic Cloud Cepheid Standards Provide a 1% Foundation for the Determination of the Hubble Constant and Stronger Evidence for Physics beyond Λ CDM*, *Astrophys. J.* **876** (2019) 85 [[1903.07603](#)].
- [11] DES collaboration, *Dark Energy Survey Year 1 Results: A Precise H_0 Estimate from DES Y1, BAO, and D/H Data*, *Mon. Not. Roy. Astron. Soc.* **480** (2018) 3879 [[1711.00403](#)].
- [12] K.C. Wong et al., *H0LiCOW XIII. A 2.4% measurement of H_0 from lensed quasars: 5.3 σ tension between early and late-Universe probes*, [1907.04869](#).
- [13] D. Pesce et al., *The Megamaser Cosmology Project. XIII. Combined Hubble constant constraints*, *Astrophys. J. Lett.* **891** (2020) [[2001.09213](#)].

- [14] C.D. Huang, A.G. Riess, W. Yuan, L.M. Macri, N.L. Zakamska, S. Casertano et al., *Hubble space telescope observations of mira variables in the sn ia host ngc 1559: An alternative candle to measure the hubble constant*, *The Astrophysical Journal* **889** (2020) 5.
- [15] W.L. Freedman, B.F. Madore, D. Hatt, T.J. Hoyt, I.S. Jang, R.L. Beaton et al., *The carnegie-chicago hubble program. viii. an independent determination of the hubble constant based on the tip of the red giant branch*, *The Astrophysical Journal* **882** (2019) 34.
- [16] L. Verde, T. Treu and A.G. Riess, *Tensions between the Early and the Late Universe*, in *Nature Astronomy 2019*, 2019, DOI [[1907.10625](https://doi.org/10.1038/s41586-019-1062-5)].
- [17] A.G. Riess, *The Expansion of the Universe is Faster than Expected*, *Nature Rev. Phys.* **2** (2019) 10 [[2001.03624](https://doi.org/10.1038/s41567-019-0362-4)].
- [18] H. Hildebrandt et al., *KiDS-450: Cosmological parameter constraints from tomographic weak gravitational lensing*, *Mon. Not. Roy. Astron. Soc.* **465** (2017) 1454 [[1606.05338](https://doi.org/10.1093/mnras/stw281)].
- [19] H. Hildebrandt et al., *KiDS+VIKING-450: Cosmic shear tomography with optical and infrared data*, *Astron. Astrophys.* **633** (2020) [[1812.06076](https://doi.org/10.1051/0004-6369/202036767)].
- [20] E. Macaulay, I.K. Wehus and H.K. Eriksen, *Lower Growth Rate from Recent Redshift Space Distortion Measurements than Expected from Planck*, *Phys. Rev. Lett.* **111** (2013) 161301 [[1303.6583](https://doi.org/10.1103/PhysRevLett.111.161301)].
- [21] B.J. Barros, L. Amendola, T. Barreiro and N.J. Nunes, *Coupled quintessence with a Λ CDM background: removing the σ_8 tension*, *JCAP* **1901** (2019) 007 [[1802.09216](https://doi.org/10.1088/1475-2875/201901/007)].
- [22] A.J. Cuesta, L. Verde, A. Riess and R. Jimenez, *Calibrating the cosmic distance scale ladder: the role of the sound horizon scale and the local expansion rate as distance anchors*, *Mon. Not. Roy. Astron. Soc.* **448** (2015) 3463 [[1411.1094](https://doi.org/10.1093/mnras/stv1294)].
- [23] P. Lemos, E. Lee, G. Efstathiou and S. Gratton, *Model independent $H(z)$ reconstruction using the cosmic inverse distance ladder*, *Mon. Not. Roy. Astron. Soc.* **483** (2019) 4803 [[1806.06781](https://doi.org/10.1093/mnras/stz1181)].
- [24] K. Aylor, M. Joy, L. Knox, M. Millea, S. Raghunathan and W.K. Wu, *Sounds Discordant: Classical Distance Ladder & Λ CDM -based Determinations of the Cosmological Sound Horizon*, *Astrophys. J.* **874** (2019) 4 [[1811.00537](https://doi.org/10.3847/1538-4357/ab0537)].
- [25] N. Arendse et al., *Cosmic dissonance: new physics or systematics behind a short sound horizon?*, *Astron. Astrophys.* **639** (2020) [[1909.07986](https://doi.org/10.1051/0004-6369/202036767)].
- [26] R.-Y. Guo, J.-F. Zhang and X. Zhang, *Can the H_0 tension be resolved in extensions to Λ CDM cosmology?*, *JCAP* **02** (2019) 054 [[1809.02340](https://doi.org/10.1088/1475-2875/201902/054)].
- [27] E. Di Valentino, A. Melchiorri and J. Silk, *Reconciling Planck with the local value of H_0 in extended parameter space*, *Phys. Lett. B* **761** (2016) 242 [[1606.00634](https://doi.org/10.1016/j.physletb.2016.06.034)].
- [28] E. Di Valentino, A. Melchiorri, E.V. Linder and J. Silk, *Constraining Dark Energy Dynamics in Extended Parameter Space*, *Phys. Rev. D* **96** (2017) 023523 [[1704.00762](https://doi.org/10.1103/PhysRevD.96.023523)].
- [29] E. Di Valentino, A. Melchiorri and J. Silk, *Cosmological constraints in extended parameter space from the Planck 2018 Legacy release*, *JCAP* **01** (2020) 013 [[1908.01391](https://doi.org/10.1088/1475-2875/202001/013)].
- [30] C.D. Kreisch, F.-Y. Cyr-Racine and O. Doré, *Neutrino puzzle: Anomalies, interactions, and cosmological tensions*, *Phys. Rev. D* **101** (2020) 123505 [[1902.00534](https://doi.org/10.1103/PhysRevD.101.123505)].
- [31] S. Vagnozzi, *New physics in light of the H_0 tension: an alternative view*, [1907.07569](https://arxiv.org/abs/1907.07569).

- [32] V. Poulin, T.L. Smith, T. Karwal and M. Kamionkowski, *Early Dark Energy Can Resolve The Hubble Tension*, *Phys. Rev. Lett.* **122** (2019) 221301 [[1811.04083](#)].
- [33] P. Agrawal, F.-Y. Cyr-Racine, D. Pinner and L. Randall, *Rock 'n' Roll Solutions to the Hubble Tension*, [1904.01016](#).
- [34] J.C. Hill, E. McDonough, M.W. Toomey and S. Alexander, *Early Dark Energy Does Not Restore Cosmological Concordance*, *Phys. Rev. D* **102** (2020) 043507 [[2003.07355](#)].
- [35] T.L. Smith, V. Poulin and M.A. Amin, *Oscillating scalar fields and the Hubble tension: a resolution with novel signatures*, *Phys. Rev. D* **101** (2020) 063523 [[1908.06995](#)].
- [36] W. Handley, *Curvature tension: evidence for a closed universe*, [1908.09139](#).
- [37] E. Di Valentino, A. Melchiorri and J. Silk, *Planck evidence for a closed Universe and a possible crisis for cosmology*, *Nat. Astron.* (2019) [[1911.02087](#)].
- [38] E. Di Valentino, A. Melchiorri and J. Silk, *Cosmic Discordance: Planck and luminosity distance data exclude LCDM*, [2003.04935](#).
- [39] S. Vagnozzi, E. Di Valentino, S. Gariazzo, A. Melchiorri, O. Mena and J. Silk, *Listening to the BOSS: the galaxy power spectrum take on spatial curvature and cosmic concordance*, [2010.02230](#).
- [40] S. Vagnozzi, A. Loeb and M. Moresco, *Eppur \ 'e piatto? The cosmic chronometer take on spatial curvature and cosmic concordance*, [2011.11645](#).
- [41] E. Di Valentino, A. Melchiorri and O. Mena, *Can interacting dark energy solve the H_0 tension?*, *Phys. Rev.* (2017) 043503 [[1704.08342](#)].
- [42] X. Li and A. Shafieloo, *A Simple Phenomenological Emergent Dark Energy Model can Resolve the Hubble Tension*, *Astrophys. J.* **883** (2019) [[1906.08275](#)].
- [43] S. Pan, W. Yang, E. Di Valentino, A. Shafieloo and S. Chakraborty, *Reconciling H_0 tension in a six parameter space?*, *JCAP* **06** (2020) 062 [[1907.12551](#)].
- [44] R.C. Nunes, *Structure formation in $f(T)$ gravity and a solution for H_0 tension*, *JCAP* **05** (2018) 052 [[1802.02281](#)].
- [45] A. El-Zant, W. El Hanafy and S. Elgammal, *H_0 Tension and the Phantom Regime: A Case Study in Terms of an Infrared $f(T)$ Gravity*, *Astrophys. J.* **871** (2019) 210 [[1809.09390](#)].
- [46] S.M. Carroll, I. Sawicki, A. Silvestri and M. Trodden, *Modified-Source Gravity and Cosmological Structure Formation*, *New J. Phys.* **8** (2006) 323 [[astro-ph/0607458](#)].
- [47] A. Awad, W. El Hanafy, G.G.L. Nashed and E.N. Saridakis, *Phase Portraits of general $f(T)$ Cosmology*, *JCAP* **1802** (2018) 052 [[1710.10194](#)].
- [48] S. Nesseris, S. Basilakos, E.N. Saridakis and L. Perivolaropoulos, *Viable $f(T)$ models are practically indistinguishable from Λ CDM*, *Phys. Rev. D* **88** (2013) 103010 [[1308.6142](#)].
- [49] S.M. Carroll, M. Hoffman and M. Trodden, *Can the dark energy equation - of - state parameter w be less than -1 ?*, *Phys. Rev.* (2003) 023509 [[astro-ph/0301273](#)].
- [50] S.M. Carroll, A. De Felice and M. Trodden, *Can we be tricked into thinking that w is less than -1 ?*, *Phys. Rev.* (2005) 023525 [[astro-ph/0408081](#)].
- [51] K.J. Ludwick, *The viability of phantom dark energy: A review*, *Mod. Phys. Lett.* (2017) [1730025](#) [[1708.06981](#)].
- [52] M. Hashim et al., *Toward a Concordance Teleparallel Cosmology II. Linear Perturbation*, in

progress (2020) .

- [53] R. Aldrovandi and J.G. Pereira, *Teleparallel Gravity*, vol. 173, Springer, Dordrecht (2013), [10.1007/978-94-007-5143-9](#).
- [54] M. Krššák, R. van den Hoogen, J. Pereira, C. Böhmer and A. Coley, *Teleparallel theories of gravity: illuminating a fully invariant approach*, *Class. Quant. Grav.* **36** (2019) 183001 [[1810.12932](#)].
- [55] Y.-F. Cai, S. Capozziello, M. De Laurentis and E.N. Saridakis, *$f(T)$ teleparallel gravity and cosmology*, *Rept. Prog. Phys.* **79** (2016) 106901 [[1511.07586](#)].
- [56] S. Camera, V.F. Cardone and N. Radicella, *Detectability of Torsion Gravity via Galaxy Clustering and Cosmic Shear Measurements*, *Phys. Rev. D* **89** (2014) 083520 [[1311.1004](#)].
- [57] R. D’Agostino and O. Luongo, *Growth of matter perturbations in nonminimal teleparallel dark energy*, *Phys. Rev. D* **98** (2018) 124013 [[1807.10167](#)].
- [58] H. Abedi, S. Capozziello, R. D’Agostino and O. Luongo, *Effective gravitational coupling in modified teleparallel theories*, *Phys. Rev. D* **97** (2018) 084008 [[1803.07171](#)].
- [59] D. Wang and D. Mota, *Can $f(T)$ gravity resolve the H_0 tension?*, *Phys. Rev. D* **102** (2020) 063530 [[2003.10095](#)].
- [60] M. Li, R.-X. Miao and Y.-G. Miao, *Degrees of freedom of $f(T)$ gravity*, *JHEP* **07** (2011) 108 [[1105.5934](#)].
- [61] R. Ferraro and M.J. Guzmán, *Hamiltonian formalism for $f(T)$ gravity*, *Phys. Rev. D* **97** (2018) 104028 [[1802.02130](#)].
- [62] M. Blagojević and J.M. Nester, *Local symmetries and physical degrees of freedom in $f(T)$ gravity: a Dirac Hamiltonian constraint analysis*, *Phys. Rev. D* **102** (2020) 064025 [[2006.15303](#)].
- [63] M.J. Guzmán and R. Ferraro, *Degrees of freedom and Hamiltonian formalism for $f(T)$ gravity*, *Int. J. Mod. Phys. A* **35** (2020) 2040022 [[1910.03100](#)].
- [64] B. Li, T.P. Sotiriou and J.D. Barrow, *$f(T)$ gravity and local Lorentz invariance*, *Phys. Rev. D* **83** (2011) 064035 [[1010.1041](#)].
- [65] T.P. Sotiriou, B. Li and J.D. Barrow, *Generalizations of teleparallel gravity and local Lorentz symmetry*, *Phys. Rev. D* **83** (2011) 104030 [[1012.4039](#)].
- [66] M. Krššák and E.N. Saridakis, *The covariant formulation of $f(T)$ gravity*, *Class. Quant. Grav.* **33** (2016) 115009 [[1510.08432](#)].
- [67] Y.-F. Cai, C. Li, E.N. Saridakis and L. Xue, *$f(T)$ gravity after GW170817 and GRB170817A*, *Phys. Rev. D* **97** (2018) 103513 [[1801.05827](#)].
- [68] M. Hohmann, M. Krššák, C. Pfeifer and U. Ualikhanova, *Propagation of gravitational waves in teleparallel gravity theories*, *Phys. Rev. D* **98** (2018) 124004 [[1807.04580](#)].
- [69] R. Ferraro and F. Fiorini, *Non trivial frames for $f(T)$ theories of gravity and beyond*, *Phys. Lett.* (2011) 75 [[1103.0824](#)].
- [70] A. Golovnev, T. Koivisto and M. Sandstad, *On the covariance of teleparallel gravity theories*, *Class. Quant. Grav.* **34** (2017) 145013 [[1701.06271](#)].
- [71] A. Golovnev and T. Koivisto, *Cosmological perturbations in modified teleparallel gravity models*, *JCAP* **1811** (2018) 012 [[1808.05565](#)].

- [72] F.K. Anagnostopoulos, S. Basilakos and E.N. Saridakis, *Bayesian analysis of $f(T)$ gravity using $f\sigma_8$ data*, *Phys. Rev. D* **100** (2019) 083517 [[1907.07533](#)].
- [73] L. Amendola et al., *Cosmology and fundamental physics with the Euclid satellite*, *Living Rev. Rel.* **21** (2018) 2 [[1606.00180](#)].
- [74] B. Li, T.P. Sotiriou and J.D. Barrow, *Large-scale structure in $f(T)$ gravity*, *Phys. Rev. D* **83** (2011) 104017 [[1103.2786](#)].
- [75] G.R. Bengochea and R. Ferraro, *Dark torsion as the cosmic speed-up*, *Phys. Rev. D* **79** (2009) 124019 [[0812.1205](#)].
- [76] E.V. Linder, *Einstein's other gravity and the acceleration of the Universe*, *Phys. Rev. D* **81** (2010) 127301 [[1005.3039](#)].
- [77] K. Bamba, C.-Q. Geng, C.-C. Lee and L.-W. Luo, *Equation of state for dark energy in $f(T)$ gravity*, *JCAP* **1101** (2011) 021 [[1011.0508](#)].
- [78] B. Xu, H. Yu and P. Wu, *Testing Viable $f(T)$ Models with Current Observations*, *Astrophys. J.* **855** (2018) 89.
- [79] SUPERNOVA SEARCH TEAM collaboration, *Observational evidence from supernovae for an accelerating universe and a cosmological constant*, *Astron. J.* **116** (1998) 1009 [[astro-ph/9805201](#)].
- [80] SUPERNOVA COSMOLOGY PROJECT collaboration, *Measurements of Ω and Λ from 42 high redshift supernovae*, *Astrophys. J.* **517** (1999) 565 [[astro-ph/9812133](#)].
- [81] D.M. Scolnic et al., *The Complete Light-curve Sample of Spectroscopically Confirmed SNe Ia from Pan-STARRS1 and Cosmological Constraints from the Combined Pantheon Sample*, *Astrophys. J.* **859** (2018) 101 [[1710.00845](#)].
- [82] SDSS collaboration, *Improved Photometric Calibration of the SNLS and the SDSS Supernova Surveys*, *Astron. Astrophys.* **552** (2013) [[1212.4864](#)].
- [83] SDSS collaboration, *Improved cosmological constraints from a joint analysis of the SDSS-II and SNLS supernova samples*, *Astron. Astrophys.* **568** (2014) [[1401.4064](#)].
- [84] J. Mosher et al., *Cosmological Parameter Uncertainties from SALT-II Type Ia Supernova Light Curve Models*, *Astrophys. J.* **793** (2014) 16 [[1401.4065](#)].
- [85] L. Amendola and S. Tsujikawa, *Dark Energy*, Cambridge University Press (2015).
- [86] BOSS collaboration, *The clustering of galaxies in the completed SDSS-III Baryon Oscillation Spectroscopic Survey: cosmological analysis of the DR12 galaxy sample*, *Mon. Not. Roy. Astron. Soc.* **470** (2017) 2617 [[1607.03155](#)].
- [87] BOSS collaboration, *The clustering of galaxies in the completed SDSS-III Baryon Oscillation Spectroscopic Survey: Observational systematics and baryon acoustic oscillations in the correlation function*, *Mon. Not. Roy. Astron. Soc.* **464** (2017) 1168 [[1607.03145](#)].
- [88] BOSS collaboration, *The clustering of galaxies in the completed SDSS-III Baryon Oscillation Spectroscopic Survey: baryon acoustic oscillations in the Fourier space*, *Mon. Not. Roy. Astron. Soc.* **464** (2017) 3409 [[1607.03149](#)].
- [89] M. Vargas-Magaña et al., *The clustering of galaxies in the completed SDSS-III Baryon Oscillation Spectroscopic Survey: theoretical systematics and Baryon Acoustic Oscillations in the galaxy correlation function*, *Mon. Not. Roy. Astron. Soc.* **477** (2018) 1153 [[1610.03506](#)].

- [90] F. Beutler, C. Blake, M. Colless, D.H. Jones, L. Staveley-Smith, L. Campbell et al., *The 6dF Galaxy Survey: baryon acoustic oscillations and the local Hubble constant*, *Mon. Not. Roy. Astron. Soc.* **416** (2011) 3017 [[1106.3366](#)].
- [91] A.J. Ross, L. Samushia, C. Howlett, W.J. Percival, A. Burden and M. Manera, *The clustering of the SDSS DR7 main Galaxy sample – I. A 4 per cent distance measure at $z = 0.15$* , *Mon. Not. Roy. Astron. Soc.* **449** (2015) 835 [[1409.3242](#)].
- [92] E.A. Kazin et al., *The WiggleZ Dark Energy Survey: improved distance measurements to $z = 1$ with reconstruction of the baryonic acoustic feature*, *Mon. Not. Roy. Astron. Soc.* **441** (2014) 3524 [[1401.0358](#)].
- [93] Y. Wang et al., *The clustering of the SDSS-IV extended Baryon Oscillation Spectroscopic Survey DR16 luminous red galaxy and emission line galaxy samples: cosmic distance and structure growth measurements using multiple tracers in configuration space*, [2007.09010](#).
- [94] W.J. Percival and M. White, *Testing cosmological structure formation using redshift-space distortions*, *Mon. Not. Roy. Astron. Soc.* **393** (2009) 297 [[0808.0003](#)].
- [95] C. Blake, S. Brough, M. Colless, C. Contreras, W. Couch, S. Croom et al., *The WiggleZ Dark Energy Survey: joint measurements of the expansion and growth history at $z < 1$* , *Mon. Not. Roy. Astron. Soc.* **425** (2012) 405 [[1204.3674](#)].
- [96] C. Howlett, A. Ross, L. Samushia, W. Percival and M. Manera, *The clustering of the SDSS main galaxy sample – II. Mock galaxy catalogues and a measurement of the growth of structure from redshift space distortions at $z = 0.15$* , *Mon. Not. Roy. Astron. Soc.* **449** (2015) 848 [[1409.3238](#)].
- [97] F. Beutler, C. Blake, M. Colless, D.H. Jones, L. Staveley-Smith, G.B. Poole et al., *The 6dF Galaxy Survey: ≈ 0 measurements of the growth rate and σ_8* , *Mon. Not. Roy. Astron. Soc.* **423** (2012) 3430 [[1204.4725](#)].
- [98] K. Said, M. Colless, C. Magoulas, J.R. Lucey and M.J. Hudson, *Joint analysis of 6dFGS and SDSS peculiar velocities for the growth rate of cosmic structure and tests of gravity*, *Mon. Not. Roy. Astron. Soc.* (2020) [[2007.04993](#)].
- [99] R.J. Cooke, M. Pettini and C.C. Steidel, *One Percent Determination of the Primordial Deuterium Abundance*, *Astrophys. J.* **855** (2018) 102 [[1710.11129](#)].
- [100] D. Blas, J. Lesgourgues and T. Tram, *The Cosmic Linear Anisotropy Solving System (CLASS). Part II: Approximation schemes*, *JCAP* **2011** (2011) 034 [[1104.2933](#)].
- [101] B. Audren, J. Lesgourgues, K. Benabed and S. Prunet, *Conservative constraints on early cosmology with MONTE PYTHON*, *JCAP* **2013** (2013) 001 [[1210.7183](#)].
- [102] A. Lewis, *GetDist: a Python package for analysing Monte Carlo samples*, [1910.13970](#).
- [103] D. Valcin, J.L. Bernal, R. Jimenez, L. Verde and B.D. Wandelt, *Inferring the Age of the Universe with Globular Clusters*, [2007.06594](#).
- [104] K.C. Schlafman, I.B. Thompson and A.R. Casey, *An Ultra Metal-poor Star Near the Hydrogen-burning Limit*, *Astrophys. J.* **867** (2018) 98 [[1811.00549](#)].
- [105] R. Jimenez, A. Cimatti, L. Verde, M. Moresco and B. Wandelt, *The local and distant Universe: stellar ages and H_0* , *JCAP* **03** (2019) 043 [[1902.07081](#)].
- [106] J. Bond, G. Efstathiou and M. Tegmark, *Forecasting cosmic parameter errors from microwave background anisotropy experiments*, *Mon. Not. Roy. Astron. Soc.* **291** (1997) L33

[[astro-ph/9702100](#)].

- [107] Y. Wang and P. Mukherjee, *Robust dark energy constraints from supernovae, galaxy clustering, and three-year wilkinson microwave anisotropy probe observations*, *Astrophys. J.* **650** (2006) 1 [[astro-ph/0604051](#)].
- [108] O. Elgaroy and T. Multamaki, *On using the CMB shift parameter in tests of models of dark energy*, *Astron. Astrophys.* **471** (2007) 65 [[astro-ph/0702343](#)].